J. Fluid Mech. (1976), *vol.* 75, *part* 2, *pp.* 287–303
Printed in Great Britain

The instability of a stratified periodic boundary layer

By CHRISTIAN VON KERCZEK

Department of Mechanical Engineering,
University of Maryland, College Park†

AND STEPHEN H. DAVIS

Department of Mechanics and Materials Science,
The Johns Hopkins University, Baltimore, Maryland 21218

(Received 15 June 1975 and in revised form 1 October 1975)

A vertical plate oscillating vertically in a statically stably-stratified fluid induces an internal wave damped by viscous forces. A two-dimensional linear stability analysis of this time-dependent state shows that the wave is highly unstable when the buoyancy and forcing frequencies are comparable. This gravitational (buoyancy) instability is due to the presence of the background stratification. The neutral curve is calculated and the system energetics are explored. Excellent agreement is obtained with the recent experimental observations of Robinson & McEwan.

1. Introduction

Consider a semi-infinite body of a density-stratified fluid with constant buoyancy frequency N bounded by a vertical plane boundary. When this rigid wall undergoes vertical harmonic oscillations with angular frequency ω, $\omega \neq N$, a periodic boundary-layer motion in the fluid results. This problem can be slightly generalized by inserting a second, stationary, plane boundary, parallel to the oscillating one. In either case exact solutions, which can be called buoyancy–Stokes layers, for the velocity and density fields of the Boussinesq equations are obtainable.

Buoyancy–Stokes layers appear (in modified form) as a result of internal wave interactions with plane boundaries that are either vertical or oblique (Wunsch 1969; Cacchione & Wunsch 1974). Thorpe (1968), McEwan (1971) and Orlanski (1972) studied finite-amplitude, forced, standing internal waves in closed containers. The growth and decay of such internal waves depends to some extent on the nature of the boundary layers at the container walls. The boundary layers at the vertical walls are of the buoyancy–Stokes type if the scale height of the density stratification is much larger than the boundary-layer thickness. It is important to know whether such boundary layers are laminar or turbulent in order to estimate the energy dissipation there. It is also important

† Present address: David W. Taylor Naval Ship Research and Development Center, Bethesda, Maryland, 20084.

to know whether an unstable disturbance in such a flow could penetrate outside the boundary layer.

The analogy between rotating and stratified flows leads one to consider similar oscillatory boundary layers in rotating flows. For example Thornley (1968) has considered Stokes layers in homogeneous incompressible rotating flows. Thus the study of such layers is relevant in several geophysical fluid mechanics applications, but the present study is restricted to vertical buoyancy–Stokes layers.

Hart (1971) has observed the buoyancy–Stokes layer on an inclined oscillating plane. For large enough oscillation amplitude, this basic flow has density inversions and so instabilities presumably associated with buoyancy effects are seen.

The experiment of Robinson & McEwan (1975) deals directly with the buoyancy–Stokes layer on a vertical wall. At no instant is there a density inversion in this basic flow yet when $\omega \approx N$, the flow is highly unstable. The secondary flow induced takes the form of regular wave motions superposed on the basic boundary-layer motion. These secondary waves can be two-dimensional, three-dimensional or a combination of these, depending on the value of $B = N/\omega$. For both $B \gg 1$ and $B \ll 1$, the basic state is highly stable.

The stability of (unstratified) Stokes layers is pertinent here. It has been investigated by von Kerzcek & Davis (1974), who found that Stokes layers are highly stable to infinitesimal disturbances. Thus it would seem that the *statically stable* stratification provides the catalyst for the instability of the buoyancy–Stokes layer.

We shall consider here the linear theory of the stability of the buoyancy–Stokes layer against two-dimensional disturbances and at high Schmidt number, $N_{Sc} = 100$. Critical values of a boundary-layer Reynolds number are obtained. In the range of B where Robinson & McEwan (1975) observed two-dimensional instability waves excellent agreement is obtained between theory and experiment. Furthermore, the eigenfunctions that correspond to these points on the neutral curve are obtained and the relevant energetics of the instability are examined. The theory does indeed show that the predicted breakdown is a buoyancy instability which results from the presence of the background stratification. The Reynolds stresses show that shear instabilities are not present. The highly unstable nature of buoyancy–Stokes layers for B near unity is due to the low rate of density diffusion, i.e. $N_{Sc} \gg 1$.

2. Formulation

Consider an incompressible Newtonian viscous fluid of density ρ' and kinematic viscosity ν confined between two infinite, vertical, parallel plates that are a distance d apart (see figure 1). Let (x', y', z') be the Cartesian co-ordinates of a system with increasing z' antiparallel to gravity, $\mathbf{g} = -g\mathbf{k}$, and $x' = 0, d$ be the positions of the plates. The corresponding velocity vector and pressure are given by (u', v', w') and p'.

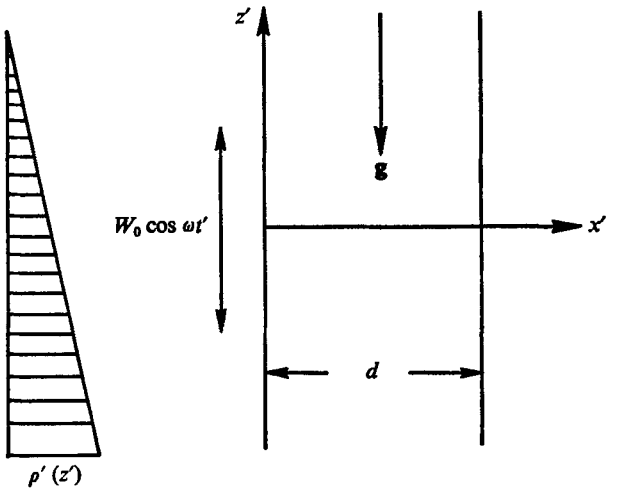

FIGURE 1. The geometry of the system. The statically stable stratification profile is indicated.

Let C' be the concentration of salt of diffusivity $\mathscr{D}$. The salt affects the local density linearly as follows:

$$\rho' = \rho_0'(1+\overline{\gamma}C'). \tag{2.1}$$

There is a background stratification, statically stable and linear, so that the background concentration C_0' satisfies

$$dC_0'/dz' = -G/\overline{\gamma} \quad (G > 0). \tag{2.2}$$

The departures from this static state are assumed to satisfy the Boussinesq equations:

$$\left.\begin{aligned} \mathbf{v}_{t'}' + \mathbf{v}'.\nabla\mathbf{v}' &= -\rho_0'^{-1}\nabla p' + \nu\nabla^2\mathbf{v}' - \overline{\gamma}gC'\mathbf{k}, \\ C_{t'}' + \mathbf{v}'.C' &= \mathscr{D}\nabla^2 C' + (G/\overline{\gamma})\,w', \\ \nabla.\mathbf{v}' &= 0. \end{aligned}\right\} \tag{2.3}$$

The basic state consists of the motion induced by the oscillation in the z' direction of the plate at $x' = 0$ with the velocity $W_0\cos\omega t'$. Here W_0 and ω are the velocity amplitude and angular frequency of the oscillation and t' is the time. The plate at $x' = d$ is stationary. The problem is scaled by introducing the following non-dimensional variables:

$$\left.\begin{aligned} t &= \omega t', \quad (x,y,z) = (x',y',z')/\delta_1, \\ \mathbf{v} &= (u,v,w) = (u',v',w')/W_0, \\ C &= (\overline{\gamma}g/\omega W_0)\,C', \quad p = p'/(\tfrac{1}{2}\rho_0'\omega W_0\delta_1), \end{aligned}\right\} \tag{2.4}$$

where

$$\delta_1 = |1-B^2|^{-\frac{1}{2}}\delta, \quad \delta = (2\nu/\omega)^{\frac{1}{2}}, \quad B = N/\omega, \quad N = (gG)^{\frac{1}{2}}.$$

Here δ is the Stokes-boundary-layer thickness and N is the buoyancy frequency of the stratification. The full fields $(0, 0, \overline{W}(x,t))$ and $\overline{C}(x,t)$ of the basic state

can be obtained exactly, given appropriate boundary conditions. It is sufficient for our purposes to display here only the large Schmidt number limit,

$$N_{Sc} = \nu/\mathscr{D} \to \infty.$$

The vertical velocity is

$$\overline{W}(x,t) = \mathrm{Re}\left\{\frac{\sinh\gamma(\beta_1 - x)}{\sinh\gamma\beta_1}\, e^{it}\right\} \tag{2.5a}$$

and the salinity excess over the stratification is

$$\overline{C}(x,t) = \mathrm{Re}\left\{\frac{-i\sinh\gamma(\beta_1 - x)}{\sinh\gamma\beta_1}\, e^{it}\right\}. \tag{2.5b}$$

Here $\beta_1 = d/\delta_1$ and $\gamma = 1 - i\,\mathrm{sgn}\,(B^2 - 1)$.

The basic state has a boundary-layer character with δ_1 measuring the spatial scale. When the stratification becomes small, $B \to 0$, so $\delta_1 \to \delta$ and the Stokes layer (von Kerczek & Davis 1974) is recovered. At $B = 1$, there is a transition from outward propagation, $B < 1$, to inward propagation, $B > 1$, of the wave-like motion. The basic state (2.5) has a limiting form for large separation, $\beta_1 \to \infty$:

$$\begin{Bmatrix}\overline{W}(x,t)\\ \overline{C}(x,t)\end{Bmatrix} = \begin{Bmatrix}\cos\,(t - \mathrm{sgn}\,(1-B^2)\,x)\\ \sin\,(t - \mathrm{sgn}\,(1-B^2)\,x)\end{Bmatrix} e^{-x}, \tag{2.6}$$

which presumably approximates well the experimental situation of Robinson & McEwan (1975).

3. Disturbances

Let the basic state for *arbitrary* Schmidt number be slightly disturbed as follows:

$$(\mathbf{v}, C, p) = (\overline{\mathbf{v}}, \overline{C}, 0) + (\mathbf{v}', C', p').$$

If this disturbed flow is substituted (with primes dropped) into the Boussinesq equations (2.3) scaled as in (2.4), then the *linearized* disturbance equations take the form

$$\begin{aligned} &2(u,v,w)_t + R^{\delta_1}(\overline{W}u_z, \overline{W}v_z, \overline{W}w_z + \overline{W}_x u)\\ &\quad = -(p_x, p_y, p_z) + |1-B^2|\,\nabla^2(u,v,w) - 2B^2(0,0,C), \end{aligned} \tag{3.1a}$$

$$2C_t + R^{\delta_1}(\overline{W}C_z + \overline{C}_x u) - 2w = |1-B^2|\,N_{Sc}^{-1}\nabla^2 C, \tag{3.1b}$$

$$u_x + v_y + w_z = 0, \tag{3.1c}$$

where

$$R^{\delta_1} = |1-B^2|\,(W_0\delta_1/\nu) = |1-B^2|^{\frac{1}{2}} R^{\delta},$$
$$R^{\delta} = W_0\delta/\nu$$

and

$$\nabla^2 = \partial^2/\partial x^2 + \partial^2/\partial y^2 + \partial^2/\partial z^2.$$

The boundary conditions are

$$u = v = w = 0 \quad \text{on} \quad x = 0, \beta_1 \tag{3.1d}$$

and the condition of zero salt flux at the walls,

$$C_x = 0 \quad \text{on} \quad x = 0, \beta_1. \tag{3.1e}$$

The stability problem (3.1) has a well-defined inviscid limit, obtained by allowing $\nu \to 0$ with $B \to 1$ such that $\nu|1-B^2|^{-1}$ and hence δ_1 are fixed. In this limit R^{δ_1} remains fixed and can be interpreted as a non-dimensional wave slope of a basic state. The limit $B \to 0$ with R^δ fixed reduces the problem to the (unstratified) Stokes layer, which von Kerczek & Davis (1974) have shown to be stable at least for $R^\delta < 800$, $0{\cdot}3 \leqslant \alpha \leqslant 1{\cdot}3$.

A Squire's transformation that relates two-dimensional and three-dimensional disturbances has not been found. We shall, however, confine our attention to two-dimensional disturbances since such disturbance waves have been observed by Robinson & McEwan (1975) and since the full three-dimensional problem poses such a massive numerical problem. Hence set $v \equiv 0$ and let all disturbance quantities be functions of (x, z, t) only. The continuity equation (3.1*c*) determines a stream function ψ as follows:

$$u = -\psi_z, \quad w = \psi_x. \tag{3.2}$$

Let us define normal-mode solutions as

$$(\psi(x,z,t), C(x,z,t)) = (\phi(x,t), \Gamma(x,t))\, e^{i\alpha z}. \tag{3.3}$$

If the pressure is eliminated from (3.1*a*) by cross-differentiation, then (3.1*a*, *b*) can be transformed through (3.2) and (3.3) to the following:

$$2\mathscr{L}\phi_t + i\alpha R^{\delta_1}(\overline{W}\mathscr{L}\phi - \overline{W}_{xx}\phi) = -2B^2\Gamma_x + |1-B^2|\,\mathscr{L}^2\phi, \tag{3.4a}$$

$$2\Gamma_t + i\alpha R^{\delta_1}(\overline{W}\Gamma - \bar{C}_x\phi) = |1-B^2|\,N_{Sc}^{-1}\mathscr{L}\Gamma + 2\phi_x, \tag{3.4b}$$

$$\mathscr{L} = \partial^2/\partial x^2 - \alpha^2, \tag{3.4c}$$

with the boundary conditions (3.1*d*, *e*) becoming

$$\phi = \phi_x = \Gamma_x = 0 \quad \text{on} \quad x = 0, \beta_1. \tag{3.4d}$$

If $(\phi(x,t), \Gamma(x,t))$ is a solution of system (3.4), the symmetries of the problem imply that $(\phi^*(x,\tau), \Gamma^*(x,\tau))$ is likewise a solution, where $\tau = t + \pi$ and an asterisk denotes a complex conjugate. The proof is obtained by substituting $\tau + \pi$ for t in system (3.4), taking the complex conjugate of the system and noting that $(\overline{W}(x,t), \bar{C}(x,t)) = -(\overline{W}(x,\tau), \bar{C}(x,\tau))$. The implication of this property is that, for each disturbance that represents a travelling wave propagating upwards, there is a wave of the same form propagating downwards. This allows the special case of standing waves. One expects from Floquet theory that the solutions can be represented in the form

$$(\phi(x,t), \Gamma(x,t)) = e^{\lambda t}(\hat{\phi}(x,t), \hat{\Gamma}(x,t)),$$

where $\hat{\phi}$ and $\hat{\Gamma}$ are 2π-periodic if λ is a simple eigenvalue. The symmetry property then implies that λ and λ^* are simultaneous eigenvalues. This property is precisely that valid for the Stokes layer but incorrectly stated in equation (6.1) of von Kerczek & Davis (1974).

4. Numerical solutions

Approximate solutions of the linearized disturbance equations (3.4) are sought using Galerkin's method. Write

$$\phi(x,t) = \sum_{m=1}^{M} a_m(t) f_m(\xi) \tag{4.1a}$$

and

$$\Gamma(x,t) = \tfrac{1}{2}c_0(t) + \sum_{m=1}^{M-1} c_m(t)\cos m\pi\xi, \tag{4.1b}$$

where for convenience the variable $\xi = x/\beta_1$ is used. Convergence is presumed for $M \to \infty$. Here the $\{f_m\}$ are eigenfunctions of the beam equation $f_m^{(\mathrm{iv})} = \nu_m f_m$ with $f_m = f_m' = 0$ on $\xi = 0, 1$. The $\{\nu_m\}$ are the corresponding eigenvalues. By a standard Galerkin procedure (e.g. see von Kerczek & Davis 1974) the system (3.4) is transformed into a system of ordinary differential equations for the coefficients $\{a_m\}$ and $\{c_m\}$. This system takes the form

$$\dot{\mathbf{b}} = \mathbf{A}(t)\,\mathbf{b}, \quad \mathbf{A}(t+2\pi) = \mathbf{A}(t), \tag{4.2}$$

where the transpose $\mathbf{b}^{\mathrm{T}}$ of $\mathbf{b}$ is defined by $\mathbf{b}^{\mathrm{T}} = (a_1, a_2, \ldots, a_M, c_0, c_1, \ldots, c_{M-1})$. The $2M \times 2M$ matrix is obtained from the Galerkin equations (A 1) given in the appendix.

The Floquet theorem (Coddington & Levinson 1955, p. 78) asserts that a fundamental solution matrix $\mathbf{F}(t)$ of system (4.2) that satisfies $\mathbf{F}(0) = \mathbf{I}$ has the form

$$\mathbf{F}(t) = \mathbf{P}(t)\,e^{\mathbf{C}t}, \tag{4.3}$$

where $\mathbf{P}(t)$ is 2π-periodic and $\mathbf{C}$ is a constant matrix. The eigenvalues $\{\lambda_i\}$ of $\mathbf{C}$, called Floquet exponents, are obtained from the eigenvalues $\{\mu_i\}$ of $\mathbf{F}(2\pi)$ and satisfy

$$\lambda_i = (2\pi)^{-1}\ln\mu_i \pmod{n}. \tag{4.4}$$

If λ_1 denotes that λ_i having the largest real part, then stability and instability are determined by $\mathrm{Re}\,\lambda_1 < 0$ and $\mathrm{Re}\,\lambda_1 > 0$ respectively. Let $\mathbf{b}_1(t)$ be the eigenvector associated with λ_1 and let $\mathbf{f}_1(2\pi)$ be the eigenvector of $\mathbf{F}(2\pi)$ associated with μ_1. The initial value $\mathbf{b}_1(0)$ of $\mathbf{b}_1(t)$ is given by

$$\mathbf{b}_1(0) = \mathbf{f}_1(2\pi)\exp(-2\pi\lambda_1). \tag{4.5}$$

Using the initial condition (4.5), the final value $\mathbf{b}_1(2\pi)$ must satisfy

$$\mathbf{b}_1(2\pi) = \mathbf{f}_1(2\pi). \tag{4.6}$$

The numerical integration procedure used is identical with that of von Kerczek & Davis (1974), whose relative merits are discussed in von Kerczek & Davis (1975). The integration need only be taken over the time interval $[0, \pi]$ since the symmetry property of §3 can be used to obtain $\mathbf{F}(2\pi)$ as $\mathbf{F}(2\pi) = \mathbf{F}^*(\pi)\,\mathbf{F}(\pi)$. Note that the statement $\mathbf{F}(t) = \mathbf{F}^*(t-\pi)$ on page 763 of von Kerczek & Davis (1975) is incorrect. It should read $\mathbf{F}(t) = \mathbf{F}^*(t-\pi)\,\mathbf{D}$, where $\mathbf{D}$ is a constant matrix.

R^{δ_1}	λ_1	λ_2
5	−0·0003	−0·0364
10	−0·0004	−0·0216
13	−0·0004	−0·0071
15	+0·0042	−0·0003

TABLE 1. The two principal Floquet exponents for $\alpha = 0{\cdot}5$, $B = 0{\cdot}909$

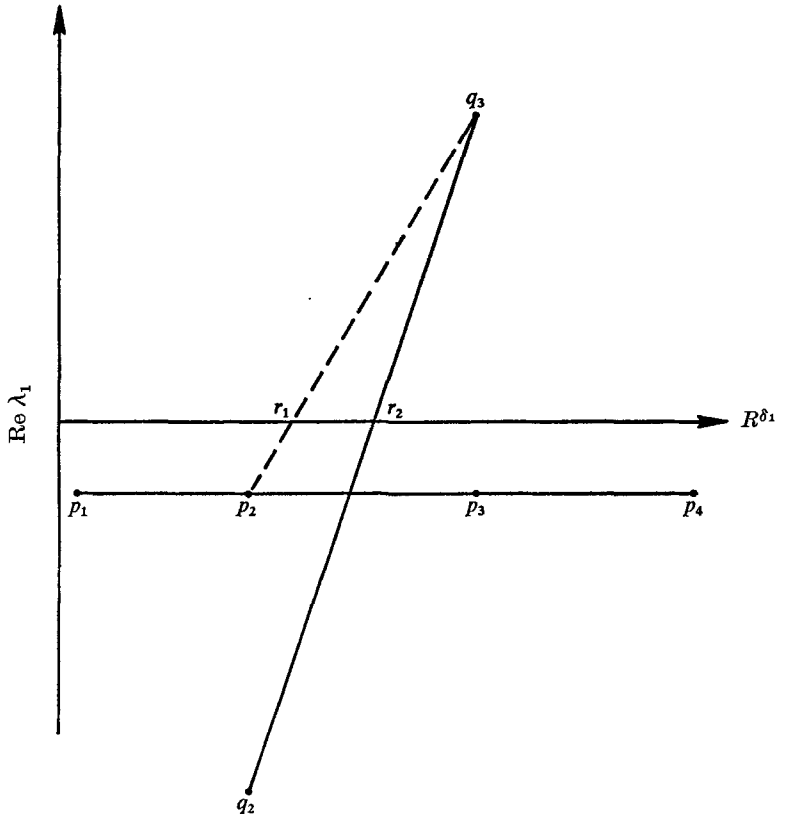

FIGURE 2. A schematic (not to scale) graph of the two principal Floquet exponents when there is seemingly modal crossing. If modal crossing is presumed, then $\lambda_1 = 0$ at $R^{\delta_1} = r_2$ is the result of linear interpolation while otherwise $R^{\delta_1} = r_1$ is obtained. The solid lines are drawn through the points p_i and q_i respectively for presumed modal crossing while the dashed line through p_2 and q_3 gives the second alternative.

Points on the neutral curve are calculated by integrating the Galerkin equations (4.2) for $N_{Sc} = 100$, $\beta_1 = 8$ and for fixed B, α and R^δ. Neutral-curve points are determined for each B by calculating λ_1 and interpolating on α and R^δ to obtain $\mathrm{Re}\,\lambda_1 = 0$. The neutral values $\mathrm{Re}\,\lambda_1 = 0$ turn out to have $\mathrm{Im}\,\lambda_1 = 0$ as well, except when $B = 1{\cdot}05$ and $0{\cdot}909$. The interpolations on R^δ for $B = 1{\cdot}05$ and $B = 0{\cdot}909$ require special mention. When the first two computed modes (the real parts of principal Floquet exponents) $p_1, p_2, \ldots$ and $q_1, q_2, \ldots$ appear to

intersect as shown in table 1 and figure 2, the neutral value $\mathrm{Re}\,\lambda_1 = 0$ is taken to be given by interpolation on the individual mode which crosses the $\mathrm{Re}\,\lambda_1 = 0$ axis, rather than on interpolation on max (p_i, q_i) for each i even though to do so might give a lower value for R_L^δ.

5. Energetics

In order to study the mechanics of the instability it is useful to examine the energetics of the disturbances. Since the disturbances are assumed periodic in z, let us define $\int_{\mathscr{V}}$ as successive integration over $z \in [0, 2\pi/\alpha]$ and $x \in [0, \beta_1]$. Hence the power integrals can be obtained by forming the inner product of (3.1a) with $\mathbf{v}$, multiplying (3.1b) by C and integrating each over $\mathscr{V}$. If the continuity condition (3.1c), the boundary conditions (3.1d, e) and Green's theorem are used, the power integrals take the form

$$2dE_k/dt = -|1-B^2|\,D_k + R^{\delta_1}\Sigma - B^2 S_V \tag{5.1a}$$

and

$$2dE_p/dt = -|1-B^2|\,N_{Sc}^{-1} D_p + R^{\delta_1} S_H + S_V, \tag{5.1b}$$

where

$$E_k = \int_{\mathscr{V}} \tfrac{1}{2}(u^2+w^2), \quad E_p = \int_{\mathscr{V}} \tfrac{1}{2}C^2,$$

$$D_k = \int_{\mathscr{V}} (|\nabla u|^2 + |\nabla w|^2), \quad D_p = \int_{\mathscr{V}} |\nabla C|^2,$$

$$S_V = \int_{\mathscr{V}} 2wC, \quad S_H = \int_{\mathscr{V}} (-uC)\,\bar{C}_x,$$

$$\Sigma = \int_{\mathscr{V}} (-uw)\,\bar{W}_x.$$

Here Σ is the production term due to Reynolds stresses and S_H is the analogous production term for salt. S_V is the volume-integrated vertical salt transport.

All quantities involved in (5.1) are evaluated using the computed eigenfunctions of the linear theory. Since linear theories contain an arbitrary multiplicative constant in each eigenfunction, a normalization is made. The quantities in (5.1) are hence relative measures. They are defined in terms of the Galerkin trial functions in the appendix.

6. Results

Points on the neutral curve have been obtained for $N_{Sc} = 100$ and $\beta_1 = 8$. These choices constitute a compromise between the desire for the large N_{Sc} and β_1 in experiment and the need for smaller values conducive to better numerical convergence. The calculations were made with the exact basic state $(\bar{W}, \bar{C})$ replaced by the $N_{Sc} \to \infty$ limiting values given in (2.5). This replacement saves a good deal of calculation, and spot checks on a related system using the exact basic state show that this approximation is, indeed, an excellent one. Bergholz

ω/N	R_L^δ	Λ_L^δ	k^δ	M
0·30	22	4	0·0006	28
0·40	21	5	0·0005	25
0·50	17	6	0·0006	24
0·65	14	8	0·0009	24
0·80	16	10	0·0006	25
0·95	18	15	0·00060	25
1·10	24	19	0·0030	25

TABLE 2. Critical conditions for various ω/N. The number M of Galerkin trial functions used and the measure k^δ of the instability growth rate according to (6.2)

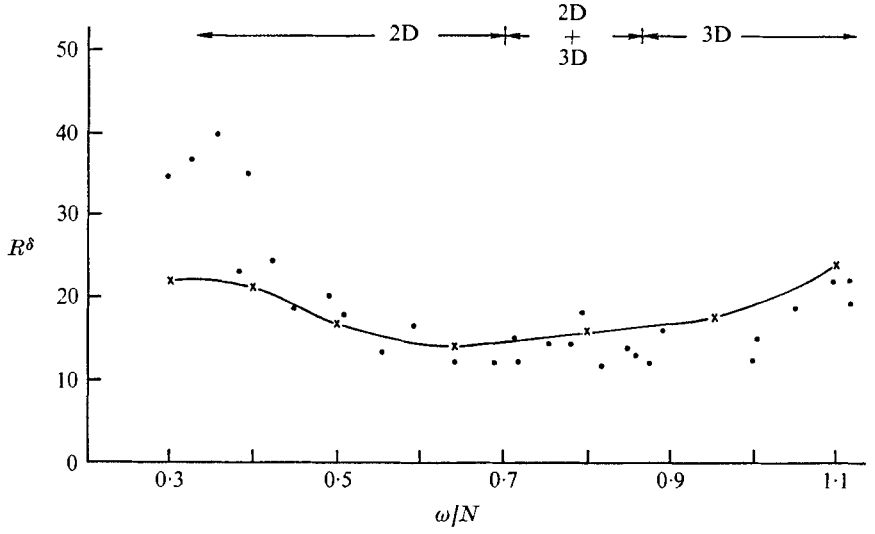

FIGURE 3. The neutral curve of R^δ *vs.* ω/N. The points are the experimental values of Robinson & McEwan (1975) for $N_{Sc} \approx 300$ while the crosses denote the results of the present two-dimensional stability theory for $N_{Sc} = 100$. The regions of two-dimensional, three-dimensional and mixed instabilities in the experiment are appropriately labelled.

(private communication, 1975) has made such checks on a similar system and has come to the same conclusion.

Table 2 lists the critical values R_L^δ of R^δ $(= (2/\omega\nu)^{\frac{1}{2}} W_0)$ obtained for various values of $B^{-1} = \omega/N$. Corresponding to R_L^δ is the wavelength of the principal two-dimensional disturbance. These critical wavelengths Λ_L^δ, scaled in units of δ, are given in table 2 with the value of M, the number of Galerkin expansion functions for each of ϕ and Γ deemed sufficient for the numerical convergence of the procedure. The accuracies of the quoted R_L^δ and Λ_L^δ are estimated to be about ± 1. The relatively large error in the latter is due to the fact that the neutral curves as a function of α are relatively flat and a more precise evaluation was deemed unnecessary.

The values of R_L^δ and Λ_L^δ are plotted in figures 3 and 4, respectively, as functions of ω/N. The dots correspond to the measured values taken from the experiment

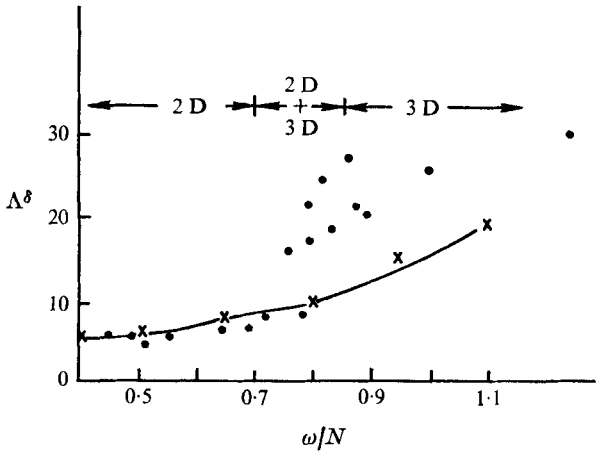

FIGURE 4. The critical Λ^δ *vs.* ω/N. The points are the experimental values of Robinson & McEwan (1975) for $N_{Sc} \approx 300$ for the vertical wavelength scaled on δ while the crosses denote the results of the present two-dimensional stability theory for $N_{Sc} = 100$.

of Robinson & McEwan (1975) for $N_{Sc} \approx 300$. These values were obtained by establishing states in which the basic flow was definitely unstable and then reducing the Reynolds number until the secondary flows seemingly vanished. They hence constitute upper bounds on the experimental critical Reynolds numbers. The crosses in these figures indicate results of the two-dimensional stability theory given herein. The regions labelled 2D, 2D + 3D and 3D are the regions where Robinson & McEwan (1975) observed instability waves of the corresponding sort. The calculated values of R_L^δ and the measured critical values (upper bounds) are in excellent agreement in the region where two-dimensional disturbances were observed. They are even in good agreement in the region where a mixture of two-dimensional and three-dimensional disturbances was observed. Where only three-dimensional disturbances were observed, the predictions of R_L^δ from our two-dimensional theory are, as expected, somewhat too high, but not startlingly so. As mentioned, the calculated z wavelength Λ_L^δ and measured Λ^δ values are not expected to agree very well but still the agreement is heartening. There is an increase in the calculated values with ω/N, which is a trend exhibited by the measured values.

It is worth mentioning that the comparisons made above are between an experiment having a fixed d, $d \approx 22{\cdot}8$ cm, and a theory having a fixed β_1, $\beta_1 = 8$. It is expected that β_1 is effectively infinite as long as δ_1 is very much smaller than d. Clearly, $\delta_1 \to \infty$ as $B \to 1$. However, with the given experimental value of d, it turns out that β_1 and d only become comparable in the approximate range $0{\cdot}99 < B < 1{\cdot}01$. None of the computed values lie in this range.

For $N_{Sc} = 100$, $\beta_1 = 8$ and a given ω/N, the eigenfunctions ψ and C corresponding to a point (α_L, R_L^δ) on the neutral curve can be calculated by first calculating the corresponding vector $\mathbf{b}_1$. (Note that Galerkin's method usually gives approximate eigenvalues much more accurately than the corresponding eigenfunctions.) The energetics of this principal mode can then be examined.

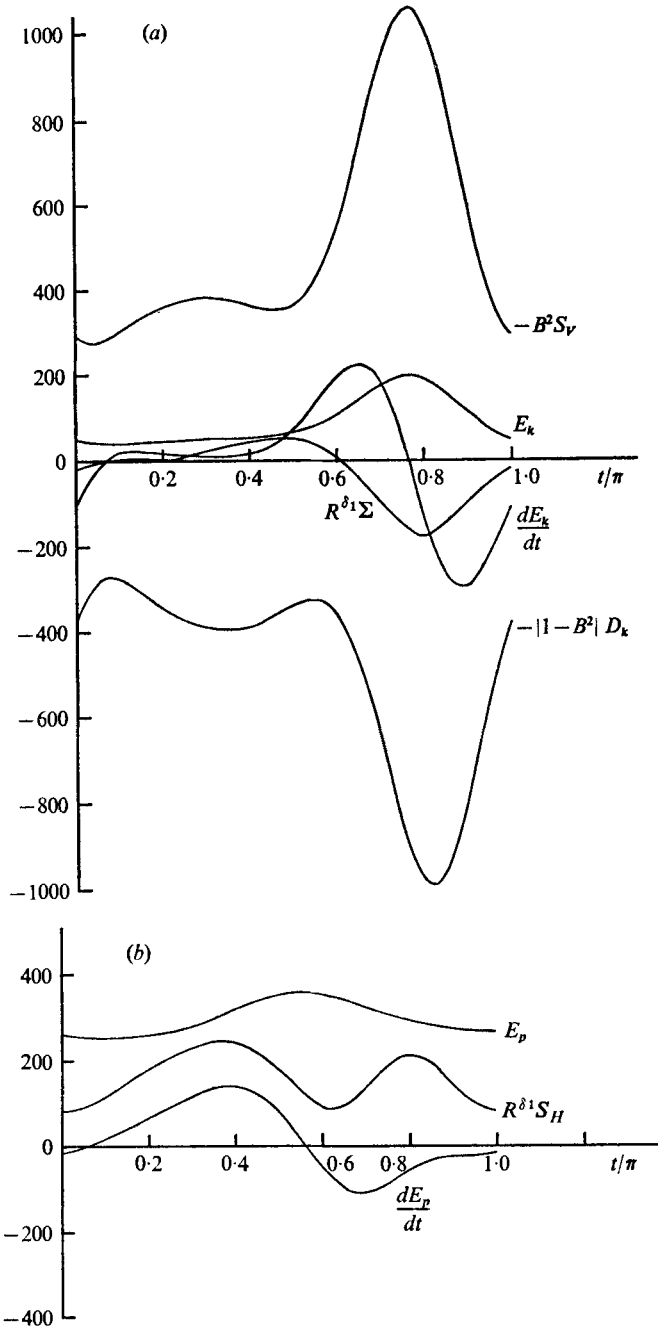

FIGURE 5. (*a*) The time evolution of the elements of the power integral (5.1*a*) for $\omega/N = 0{\cdot}5$, $\alpha = 0{\cdot}6$ for neutral stability. The algebraic sum of $-|1-B^2|\,D_k$, $R^{\delta_1}\Sigma$ and $-B^2S_V$ gives the rate of increase of the disturbance kinetic energy E_k. (*b*) The time evolution of the elements of the power integral (5.1*b*) for $\omega/N = 0{\cdot}5$, $\alpha = 0{\cdot}6$ for neutral stability. The dissipation term containing D_p is omitted since it is very small. The algebraic sum of $R^{\delta_1}S_H$, S_V [see (*a*)] and $-|1-B^2|\,N_{Sc}^{-1}\,D_p$ gives the rate of increase of the disturbance potential energy E_p.

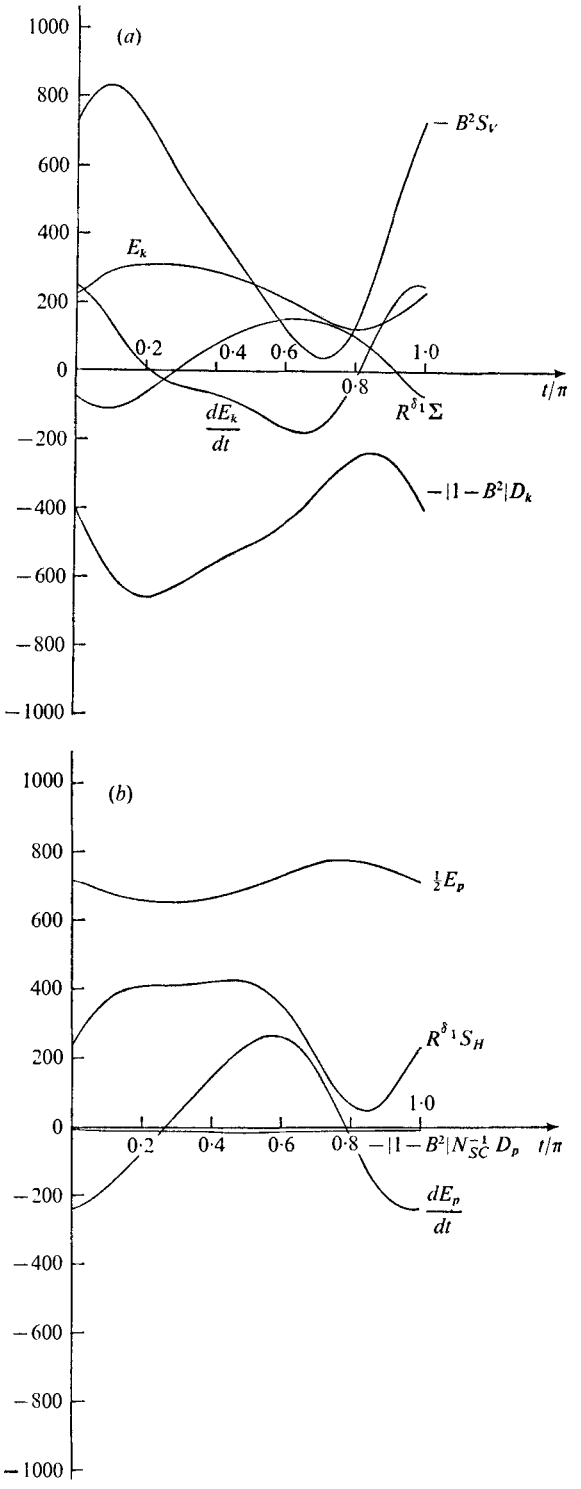

FIGURE 6. (*a*) The time evolution of the elements of the power integral (6.1*a*) for $\omega/N = 0{\cdot}8$, $\alpha = 0{\cdot}8$ for neutral stability. The algebraic sum of $-|1-B^2|\ D_k$, $R^{\delta_1}\Sigma$ and $-B^2S_V$ gives the rate of increase of the disturbance kinetic energy E_k. (*b*) The time evolution of the elements of the power integral (6.1*b*) for $\omega/N = 0{\cdot}8$, $\alpha = 0{\cdot}8$ for neutral stability. The algebraic sum of $R^{\delta_1}S_H$, S_V [see (*a*)] and $-|1-B^2|\ N_{Sc}^{-1}\ D_p$ gives the rate of increase of the disturbance potential energy E_p. Notice the different scale for E_p.

By computing every term in the power integrals (5.1), one can make a consistency test on the numerical procedures used. Several such tests were made at various times t. In each case (5.1) gave identities to three decimal places. The values of E_k, E_p, D_k, D_p, S_V, S_H and Σ for $t = 0$ and $t = \pi$ are compared and on the neutral curve, the values agree to four significant figures. Finally, the strongest test compares the Galerkin eigenfunction $\mathbf{b}_1(2\pi)\, e^{-2\pi\lambda_1}$ with $\mathbf{b}_1(0)$ as given in (4.6). Such comparisons give equality to four-figure accuracy. Figures 5 and 6 illustrate the time dependence of each term in (5.1) on the neutral curve at $\omega/N = 0{\cdot}5$ and $0{\cdot}8$, respectively. Figures 5(*a*) and 6(*a*) compare the terms in (5.1*a*) and show that the viscous dissipation $-|1-B^2|\,D_k$ is strongly negative while the vertical salt transport $-B^2S_V$ is always positive but has a tall peak value in each case. The 'Reynolds stress' production term is always a relatively small contributor, showing that shear-flow instabilities are not a danger. The algebraic sum of the three curves gives dE_k/dt. E_k can be inferred or it can be computed directly. These figures show that changes in ω/N result in shifts of the curves and rather different behaviours in each case. The terms in (5.1*b*) are illustrated in figures 5(*b*) and 6(*b*) for the same values of ω/N. Since the Schmidt number is so large, the dissipation is extremely small in magnitude. In fact, it is so small for $\omega/N = 0{\cdot}5$ that it has been omitted from figure 5(*b*). The vertical salt transport can be obtained from figures 5(*a*) and 6(*a*) by the division of $-B^2S_V$ by $-B^2$. The algebraic sum is dE_p/dt. E_p can be inferred or it can be computed directly. Again, changes in ω/N result in shifts and modifications in the curves. There is a strong correlation between the vertical salt transport and the behaviour of the disturbance kinetic energy E_k. The peaks in the disturbance potential energy E_p are shifted with ω/N. However, these distributions should be compared with the following statement from Robinson & McEwan (1975) of their observations using a schlieren system: "On the upward stroke the disturbance became visible just before the top of the stroke [$t = \frac{1}{2}\pi$]...The disturbance amplitude, determined by the degree of contrast in the schlieren image between crests and troughs, reached a maximum at about [$t = \frac{3}{4}\pi$], after which it decreased and became no longer visible at about [$t = \pi$], i.e. at zero displacement of the oscillating wall...The evolution was repeated in a similar manner during the other half of the stroke from [$t = \pi$] to [$t = 2\pi$]." The present predictions roughly reproduce such details and give us confidence that the present linear theory captures the essential physics of the instability process.

In the neighbourhood of the neutral curve, the real part $\mathrm{Re}\,\lambda_1$ of the Floquet exponent, which is the growth rate of the disturbance scaled on ω, should be representable as follows:

$$\mathrm{Re}\,\lambda_1 = k^\delta(R^\delta - R_L^\delta) + O((R^\delta - R_L^\delta)^2) \tag{6.1}$$

as $R^\delta \to R_L^\delta$. Hence the determination of k^δ gives a measure of the growth rate of the disturbance. It follows from (6.1) that

$$k^\delta = \frac{d}{dR^\delta}(\mathrm{Re}\,\lambda_1)\big|_{R^\delta = R_L^\delta}. \tag{6.2}$$

Table 2 lists *rough* estimates of k^δ as a function of B obtained b linearly interpolating the numerical values of $\mathrm{Re}\,\lambda_1$ near $R = R_L^\delta$.

R^δ	Re λ_1
12	$-2{\cdot}9 \times 10^{-2}$
19	$4{\cdot}0 \times 10^{-3}$
25	$5{\cdot}1 \times 10^{-2}$
31	$1{\cdot}0 \times 10^{-1}$
38	$1{\cdot}4 \times 10^{-1}$

TABLE 3. The principal Floquet exponent Re λ_1 for various R^δ for $\alpha_L = 1{\cdot}25$, $B = 1{\cdot}05$

Finally, table 3 presents the values of λ_1 for $B = 1{\cdot}05$ and $\alpha_L^\delta = 1{\cdot}25$ at a variety of values of R^δ.

7. Discussion

The computations for the neutral curve show that, as in the experiment by Robinson & McEwan (1975), the buoyancy–Stokes layer is highly stable for both $\omega/N \gg 1$ and $\omega/N \ll 1$. In the former case, the stratification is negligibly small, so that the flow is approximately an (unstratified) Stokes layer, which von Kerzcek & Davis (1974) have shown to be stable for $R^\delta < 800$, $0{\cdot}3 \leqslant \alpha \leqslant 1{\cdot}3$ and $\beta = \beta_1 = 8$. The two-dimensional disturbances considered were sufficient since a version of Squire's theorem was proved. In the latter case the stratification is strong, so that the characteristic Reynolds number of the flow is R^{δ_1} rather than R^δ. Figure 3 shows that, for ω/N down to 0·3, a rather flat neutral curve (in terms of R^δ) is predicted but since $R^{\delta_1} \sim BR^\delta$ as $B \to \infty$, this flow is highly stable in terms of R^{δ_1} for small ω. It is only for intermediate values of ω/N that an instability might be prominent. In this case, the oscillating plate causes instantaneous horizontal density gradients which lead to a local buoyancy instability, as seen in figures 5 and 6, only if the density diffusion is too small to erase the differences. Hence this buoyancy instability is a large Schmidt number event. The presence of the background stratification gives rise to the instability and since ω and N are comparable, the growth rates of the instability scale on N. For intermediate values of ω/N, the buoyancy–Stokes layer is unstable at R^δ in the range 10–20. The inviscid limit (see §3) of the problem is considered, i.e. $\nu \to 0$, $B \to 1$ such that R^{δ_1} remains fixed; the limiting form of R^{δ_1} represents the slope of an inviscid wavelike (exponentially decreasing with x) basic state. Inviscid, *constant amplitude* states can be shown to be susceptible to parametric subharmonic forcing (McEwan & Robinson 1975) by large-scale wave fields or to small-scale wave fields (Bretherton 1974, private communication) rendering the basic-state wave unstable.

The instabilities considered are manifest on a boundary layer whose thickness is $O(\delta_1)$. Figures 7(*a*) and (*b*) show the structure of the z-averaged kinetic and potential energies, $e_k(x,t)$ and $e_p(x,t)$, respectively, for a particular case,

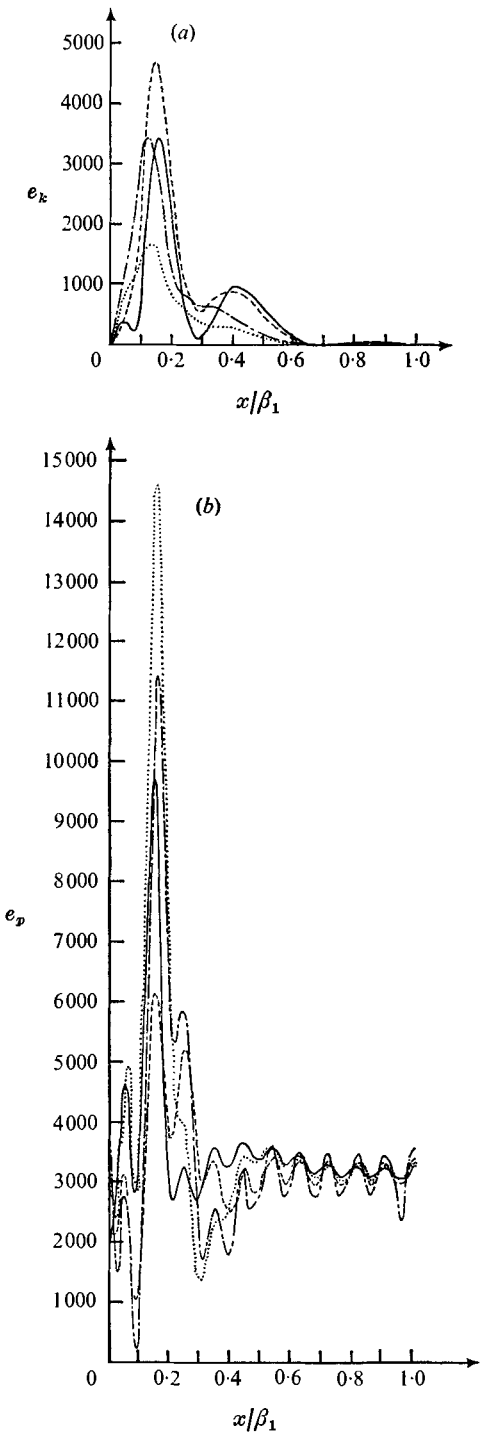

FIGURE 7. The structure functions (*a*) $e_k(x, t)$ and (*b*) $e_p(x, t)$ at various times for the case $\alpha = 0{\cdot}8$, $R^\delta = 16$, $\omega/N = 0{\cdot}8$ and $\beta_1 = 8$; Re $\lambda_1 \approx -1 \times 10^{-4}$. ——, $t = 0$; - - - -, $t = \frac{1}{4}\pi$; – – –, $t = \frac{1}{2}\pi$; ·····, $t = \frac{3}{4}\pi$. In (*b*) the oscillations for large x are presumably due to the fact that the eigenfunctions are approximated more poorly than the corresponding eigenvalues.

$\omega/N = 0{\cdot}8$, $\alpha = 0{\cdot}8$ and $R^\delta = 16$. These energies are defined implicitly as follows:

$$E_k(t) = \int_0^{\beta_1} e_k(x,t)\,dx, \quad E_p(t) = \int_0^{\beta_1} e_p(x,t)\,dx.$$

They show that even though the critical wavelength (see table 2) $\Lambda^\delta = 10$ is $7{\cdot}5$ times δ_1, the effective depth of penetration of this critical disturbance is only two or three times δ_1.

The authors are grateful for the partial support of the National Science Foundation through Grants GK-39933X (Applied Mathematics) and GA-35390X (Atmospheric Sciences). The computations were done at the National Center for Atmospheric Research, which is supported by the National Science Foundation. Mr R. Bergholz, Department of Engineering Mechanics, University of Michigan, kindly made some numerical checks for us and made his results available to us. Prof. J. Pedlosky made thoughtful comments on an earlier version of this work.

Appendix

The Galerkin approximation equations are as follows:

$$\dot{a}_m(t) = \tfrac{1}{2}\beta_1^{-2}\,|1-B^2|\,Q_{ml}^{-1}P_{ln}a_n - \tfrac{1}{2}i\bar{\alpha}\beta_1^{-1}R^{\delta_1}Q_{ml}^{-1}V_{ln}a_n - B^2Q_{ml}^{-1}T_{ln}c_n \quad (m = 1,2,\ldots,M), \quad \text{(A 1}a\text{)}$$

$$\dot{c}_0(t) = -\tfrac{1}{2}|1-B^2|\,\beta_1^{-2}\bar{\alpha}^2c_0 - i\bar{\alpha}\beta_1^{-1}R^{\delta_1}(\tfrac{1}{2}W_{00}c_0 + W_{0m}c_0 - U_{0m}a_m), \quad \text{(A 1}b\text{)}$$

$$\delta_{mn}\dot{c}_m(t) = -\tfrac{1}{2}|1-B^2|\,\beta_1^{-2}(n^2\pi^2+\bar{\alpha}^2)\,c_m\delta_{mn} - i\bar{\alpha}\beta_1^{-1}R^{\delta_1}(\tfrac{1}{2}W_{n0}c_0 + W_{nm}c_0 - U_{nm}a_m) - 2T_{mn}a_m \quad (n = 1,2,\ldots,M-1), \quad \text{(A 1}c\text{)}$$

where $\bar{\alpha} = \beta_1\alpha$ and the summation convention holds.

$$Q_{mn} = \langle\bar{\mathscr{L}}f_n, f_m\rangle, \quad P_{mn} = \langle\bar{\mathscr{L}}^2f_n, f_m\rangle,$$
$$V_{mn} = \langle\overline{W}\bar{\mathscr{L}}f_n, f_m\rangle - \langle\overline{W}_{\xi\xi}f_n, f_m\rangle,$$
$$T_{mn} = -n\pi\langle\sin n\pi\xi, f_m\rangle,$$
$$W_{mn} = \langle\overline{W}\cos n\pi\xi, \cos m\pi\xi\rangle, \quad U_{mn} = \langle\bar{C}_\xi f_n, \cos m\pi\xi\rangle,$$

where

$$\bar{\mathscr{L}} = \partial^2/\partial\xi^2 - \alpha^2, \quad \langle f,g\rangle \equiv \int_0^1 f(\xi)\,g(\xi)\,d\xi.$$

The Galerkin expressions for the elements of the power integrals are as follows:

$$E_k = -\tfrac{1}{2}\beta_1^2Q_{mn}a_na_m^*, \quad E_p = \tfrac{1}{8}\beta_1^2(c_0c_0^* + 2c_nc_n^*),$$
$$D_k = -\tfrac{1}{4}P_{mn}(a_m^*a_n + a_ma_n^*),$$
$$D_p = -\tfrac{1}{8}(\bar{\alpha}^2c_0c_0^* + 2(m^2\pi^2+\bar{\alpha}^2)\,c_mc_m^*),$$
$$S_V = -\tfrac{1}{2}\beta_1^2T_{nm}(c_ma_n^* + c_m^*a_n),$$
$$S_H = \tfrac{1}{8}i\bar{\alpha}\beta_1[U_{0n}(c_0^*a_n - c_0a_n^*) + 2U_{mn}(c_m^*a_n - c_ma_n^*)],$$
$$\Sigma = \tfrac{1}{4}i\bar{\alpha}\beta_1(V_{mn} - V_{nm})\,a_na_m^*.$$

REFERENCES

CACCHIONE, D. & WUNSCH, C. 1974 Experimental study of internal waves over a slope. *J. Fluid Mech.* **66**, 223.

CODDINGTON, E. A. & LEVINSON, N. 1955 *Theory of Ordinary Differential Equations.* McGraw-Hill.

HART, J. E. 1971 A possible mechanism for boundary layer mixing and layer formation in a stratified fluid. *J. Phys. Ocean.* **1**, 258.

KERCZEK, C. VON & DAVIS, S. H. 1974 Linear stability theory of oscillatory Stokes layers. *J. Fluid Mech.* **62**, 753.

KERCZEK, C. VON & DAVIS S. H. 1975 Calculation of transition matrices. *A.I.A.A. J.* **13**, 1400.

MCEWAN, A. D. 1971 Degeneration of resonantly-excited standing internal gravity waves. *J. Fluid Mech.* **50**, 431.

MCEWAN, A. D. & ROBINSON, R. M. 1975 Parametric instability of internal waves. *J. Fluid Mech.* **67**, 667.

ORLANSKI, I. 1972 On the breaking of standing internal gravity waves. *J. Fluid Mech.* **54**, 577.

ROBINSON, R. M. & MCEWAN, A. D. 1975 Instability of a periodic boundary layer in a stratified fluid. *J. Fluid Mech.* **68**, 41.

THORNLEY, C. 1968 On Stokes and Rayleigh layers in a rotating system. *Quart. J. Mech. Appl. Math.* **21**, 451.

THORPE, S. A. 1968 On standing internal gravity waves of finite amplitude. *J. Fluid Mech.* **32**, 489.

WUNSCH, C. 1969 Progressive internal waves on slopes. *J. Fluid Mech.* **35**, 131.